ELSEVIER

Ceramics International 30 (2004) 2269–2275

CERAMICS INTERNATIONAL

www.elsevier.com/locate/ceramint

Microstructures and mechanical properties of 8Y-FSZ ceramics with $BaTiO_3$ additive

X.Q. Liu, X.M. Chen*

Department of Materials Science and Engineering, Zhejiang University, Hangzhou 310027, China

Received 5 September 2003; received in revised form 13 November 2003; accepted 7 January 2004
Available online 26 April 2004

Abstract

The microstructure and mechanical properties of 8 mol% Y_2O_3 fully stabilized zirconia (8Y-FSZ) with $BaTiO_3$ additive were investigated. The introduction of $BaTiO_3$ additive would significantly increase the density and the grain size of 8Y-FSZ ceramics. XRD, Raman spectroscopy, and dielectric measurement were performed. A rhombohedral $Ba(Ti_{1-x}Zr_x)O_3$ ferroelectric phase resulted in the composite with 5 mol% additive, while for those with higher additive content, the secondary phase changes to cubic $Ba(Ti_{1-x}Zr_x)O_3$. The fracture toughness of the $x BaTiO_3/(1-x)$8Y-FSZ composites reached a maximum and then decreased with increasing the amount of additive. The highest value reached 6.1 MPa $m^{1/2}$ for $0.05BaTiO_3/0.95$(8Y-FSZ) sintered at 1475 °C for 3 h, where the piezoelectric/ferroelectric secondary phase toughening played an important role. Moreover, the fracture toughness of the composites increased firstly and then decreased with increasing sintering temperature.

Keywords: B. Composite; C. Toughness and toughening; D. ZrO_2; Piezoelectric secondary phase toughening

1. Introduction

Toughening is a very important issue for ceramics. During the past two decades, a serial of toughening approaches have been proposed and developed [1,2]. Recently, Chen and coworkers have proposed a new toughening method [3–5], in which a piezoelectric and/or ferroelectric secondary phase was introduced into ceramic matrix as toughening agent and the energy dissipation and/or conversion due to domain wall motion and piezoelectric effect were considered as a new toughening mechanism. Some other groups also showed their interests in this method [6–9]. The so-called piezoelectric/ferroelectric secondary phase toughening approach was successfully applied in the systems: $BaTiO_3/Al_2O_3$ [3,8], $Nd_2Ti_2O_7/Al_2O_3$ [4], $Sr_2Nb_2O_7$/3Y-TZP [5,10], $LiTaO_3/Al_2O_3$ [6,7], glass/PZT [9], $Sr_2Nb_2O_7$/ZTA [11], and $Sr_2Nb_2O_7/LaAlO_3$ [12].

On the other hand, fully stabilized zirconia with 8 mol% Y_2O_3 (8Y-FSZ) has been widely used in solid state fuel cell (SOFC) and oxygen sensor because of its high oxygen-ion conductivity over a wide range of temperature and oxygen partial pressure [13–15]. However, the fracture toughness of 8Y-FSZ ceramics just ranges from 0.9 to 3 MPa $m^{1/2}$ according to different authors [13,16], and it is not high enough to suffer the thermal stress and the stress caused during processing. Therefore, toughening of 8Y-FSZ ceramics is a key issue in applying them as the components of SOFC and oxygen sensors. So far, some work has been performed on this topic [13,17,18]. Monoclinic zirconia has been added to toughen the 8Y-FSZ ceramics, unfortunately the addition degraded the conductivity of 8Y-FSZ ceramics to an unacceptable level for SOFC application [13]. The addition of fine particles of partially stabilized zirconia and alumina has enhanced the fracture toughness without significantly degrading the conductivity of 8Y-FSZ ceramics [13,17]. Moreover, nanosized SiC particles were selected as the reinforcement for 8Y-FSZ ceramics, and both the fracture toughness and the fracture strength were improved, while the conductivity had not been investigated [18].

In the previous work, the effects of $BaTiO_3$ upon the microstructures and mechanical properties of 3Y-TZP ceramics were investigated [19]. Because the introduction of

* Corresponding author. Tel.: +86-571-8795-2112; fax: +86-571-8795-2112.
E-mail address: xmchen@cmsce.zju.edu.cn (X.M. Chen).

0272-8842/$30.00 © 2004 Elsevier Ltd and Techna S.r.l. All rights reserved.
doi:10.1016/j.ceramint.2004.01.006

$BaTiO_3$ additive decreased the amount of transformable tetragonal zirconia in 3Y-TZP, and, therefore, decreased the toughness due to the phase transformation toughening, and this effect was greater than that of piezoelectric/ferroelectric secondary phase toughening, so the overall toughness decreased with the $BaTiO_3$ additive in 3Y-TZP ceramics. However, there is no transformable tetragonal zirconia phase in the 8Y-FSZ ceramics, and, therefore, the significant effects of piezoelectric/ferroelectric secondary phase toughening should be expected.

In the present work, $BaTiO_3$ added 8Y-FSZ ceramics are prepared, and the mechanical properties were investigated together with the microstructures. The effects of piezoelectric/ferroelectric secondary phase toughening are emphasized.

2. Experimental procedure

Reagent-grade $BaCO_3$ (99.93%) and TiO_2 (99.5%) in 1:1 mole ratio were mixed by ball milling in ethanol using zirconia media for 24 h. The slurry was dried and then calcined at 1250 °C for 3 h in air to prepare $BaTiO_3$. Then, the as-received 8Y-FSZ powders (Shenzhen Nanbo Structure Ceramics Co. Ltd.) with $BaTiO_3$ additive were mixed in the formula of $x BaTiO_3/(1-x)$8Y-FSZ ($x = 0$, 0.05, 0.10, and 0.15) by ball milling using zirconia media in ethanol for 24 h. After drying, such mixed powders were pressed into disc compacts of 12 mm in diameter and 1 to 4 mm in height, and these compacts were sintered between 1450 and 1600 °C for 3 h in air.

The microstructures were evaluated by scanning electron microscopy (SEM, HITACHI S-570), and the phase constitution of the composite ceramics was characterized by X-ray powder diffraction (XRD) analysis using Cu Kα radiation. To identify the exact $BaTiO_3$ phase in the sintered sample, Raman scattering measurement was conducted using a Raman scope (Thermo Nicolet ALMEGA Dispersive Raman) and the excitation light source was a diode pump solid state frequency doubled YAG laser ($\lambda = 532$ nm) with 30 mW of power, and the variation of dielectric constant in the temperature range from −60 to 130 °C was measured at a precious LCR meter (HP 4284A) at 10 kHz.

The effective elastic modulus was evaluated using the method proposed by Marshall et al. [20] where a diamond Knoop indenter was used combined with a diamond Vickers indenter. The results were averaged over six indentations per specimen and the following formula was used in the calculations [20]:

$$\frac{b'}{a'} = \frac{b}{a} - \frac{\alpha H}{E} \tag{1}$$

where, b'/a' and b/a were the ratio of diagonal dimensions of Knoop indentation and that of Knoop indenter, respectively, α was a constant, H was the Vickers hardness and E was the effective elastic modulus. Here, $b/a = 1/7.11$ and $\alpha = 0.45$ were used during calculating.

The fracture toughness was evaluated by the modified indentation method [21,22] at room temperature using a diamond Vickers indenter with a loading time of 15 s at a constant load of 50 N on polished surface. The results were averaged over six indentations per specimen and the following formula was used for the calculations [21,22]:

$$\left(\frac{K_{1C}\phi}{Ha^{1/2}}\right)\left(\frac{H}{E\phi}\right)^{2/5} = 0.035\left(\frac{l}{a}\right)^{-1/2} \tag{2}$$

where, K_{1C} was the toughness of the composite ceramic, H was the Vickers hardness, E was the effective elastic modulus, ϕ was the constraint factor (≈3), l was the crack length, and a was the half diagonal length of an indentation.

3. Results and discussion

The bulk densities of $x BaTiO_3/(1-x)$8Y-FSZ ceramics with various compositions are shown in Fig. 1 as a function of sintering temperature. Dense 8Y-FSZ ceramics cannot be obtained even by sintering at 1600 °C for 3 h, and the relative density is about 91%. The introduction of $BaTiO_3$ additive greatly improves the densification behavior of 8Y-FSZ ceramics. As shown in Figs. 2 and 3, the grain size increases with increasing the content of $BaTiO_3$ additive and the sintering temperature. These results show that the addition of $BaTiO_3$ additive improves the mobility of grain boundary of the 8Y-FSZ ceramics, and the higher movable grain boundary will lead to both grain size and relative density increase.

Fig. 4 shows the XRD patterns of $x BaTiO_3/(1-x)$8Y-FSZ ceramics sintered under different conditions. For $x = 0$, the single cubic phase is obtained. For samples with $BaTiO_3$ additive, the major phase is cubic zirconia, but the secondary phase cannot be identified only from the XRD patterns since the patterns of $BaTiO_3$ polymorphic phases are very similar. To exactly identify the secondary phase, Raman spec-

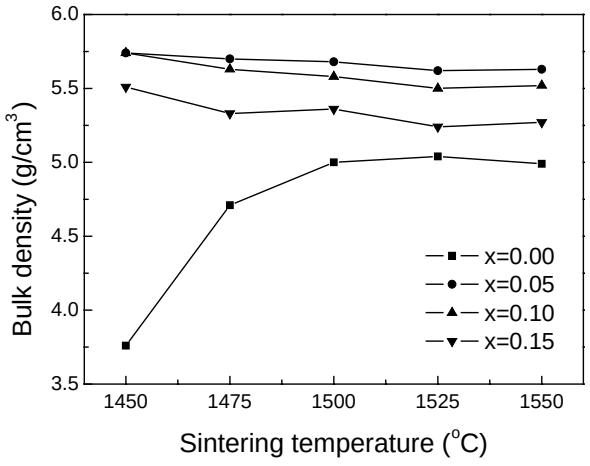

Fig. 1. Bulk densities of $x BaTiO_3/(1-x)$8Y-FSZ ceramics sintered at different temperature for 3 h.

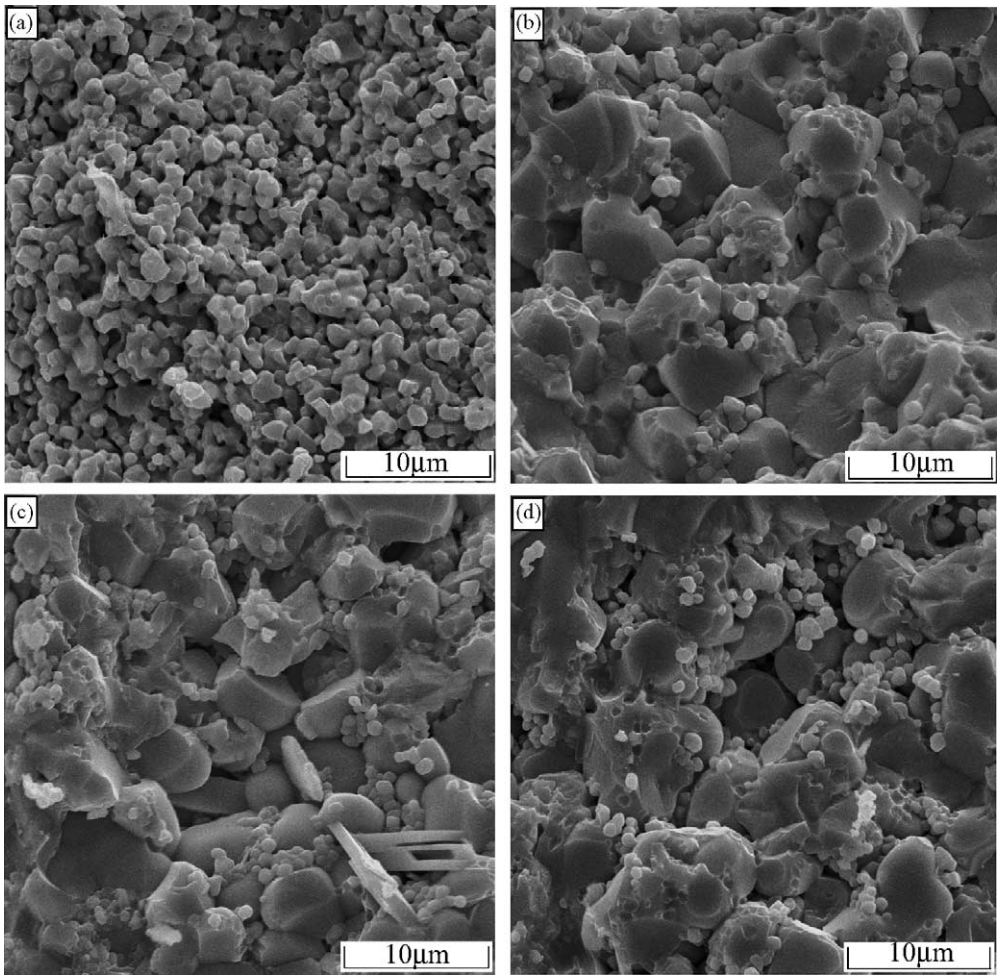

Fig. 2. SEM micrographs of xBaTiO$_3$/(1 − x)8Y-FSZ ceramics sintered at 1475 °C for 3 h: (a) $x = 0.00$; (b) $x = 0.05$; (c) $x = 0.10$; (d) $x = 0.15$.

troscopy and dielectric measurement are investigated. Fig. 5 shows the Raman spectra of xBaTiO$_3$/(1−x)8Y-FSZ ceramics sintered at 1475 °C for 3 h. The peak around 630 cm^{-1} is the characteristic peak of 8Y-FSZ [23], and a strong polarized spectrum is shown for pure 8Y-FSZ, which originated from the breakdown of wave-vector selection rules due to the structural disorder of the oxygen atoms [23]. While the spectra of 8Y-FSZ with BaTiO$_3$ additive evolves with the additive content, and the variation trend is very similar to that of Ba(Ti$_{1-x}$Zr$_x$)O$_3$ with increasing the amount of replacement [24,25]. The two ions radius being close (Ti^{4+}: 0.075 nm, Zr^{4+}: 0.085 nm), the substitution of Ti^{4+} in BaTiO$_3$ with Zr^{4+} in 8Y-FSZ is very easy. And the previous work has showed that the phase of Ba(Ti$_{1-x}$Zr$_x$)O$_3$ changed from tetragonal to orthorhombic, rhombohedral, and then cubic phase [24]. To confirm the secondary phase, the variation of the dielectric constant with temperature has been investigated and the results are shown in Fig. 6. There is no peak for 8Y-FSZ ceramics, while a broad peak around 50 °C for 0.05BaTiO$_3$/0.95(8Y-FSZ) ceramics, and a sharp peak around 0 °C for $x = 0.10$ and $x = 0.15$ in xBaTiO$_3$/(1 − x)8Y-FSZ composites are observed. There are three phase transitions of BaTiO$_3$ ceramics at $T_1 = 183$ K, $T_2 = 283$ K, and $T_c = 400$ K, and the Curie point of Ba(Ti$_{1-x}$Zr$_x$)O$_3$ ceramics decreases with increasing the Zr content, while the other two phase transition temperatures, T_1 and T_2 increases, and the three phase transitions will merge into one broad peak for $x = 0.15$ [24,25]. The Ba(Ti$_{1-x}$Zr$_x$)O$_3$ ceramic is cubic at the temperature above the broad peak, while it is rhombohedral ferroelectric phase under the peak. Combination of the results of Raman spectra and dielectric spectra, one can find that for the xBaTiO$_3$/(1 − x)8Y-FSZ composite with $x = 0.05$ the secondary phase is rhombohedral ferroelectric phase, and those composites with $x = 0.10$ and $x = 0.15$ are cubic phase at the room temperature.

The mechanical properties are shown in Table 1. For $x = 0$, when the sintering temperature is lower than 1600 °C, the mechanical properties cannot be obtained using indentation method for these very low relative densities. Even for the 8Y-FSZ sample sintered at 1600 °C for 3 h, the Young's modulus is much lower than the one reported in the literature [16] for this low relative density (about 91% T.D.), while the fracture toughness is similar to the value reported by Minh [13]. In general, the Young's modulus of xBaTiO$_3$/(1−

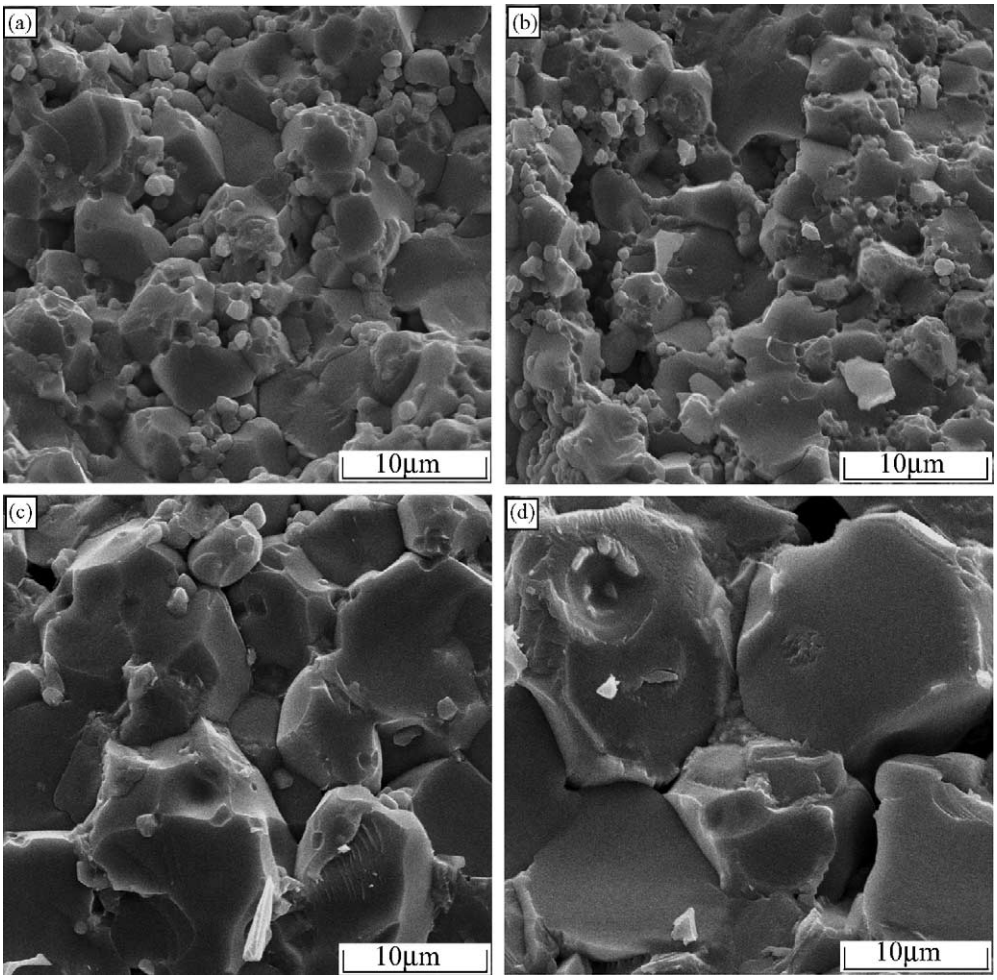

Fig. 3. SEM micrographs of $0.05BaTiO_3/0.95$(8Y-FSZ) ceramics sintered at: (a) 1475 °C/3 h; (b) 1500 °C/3 h; (c) 1525 °C/3 h; (d) 1550 °C/3 h.

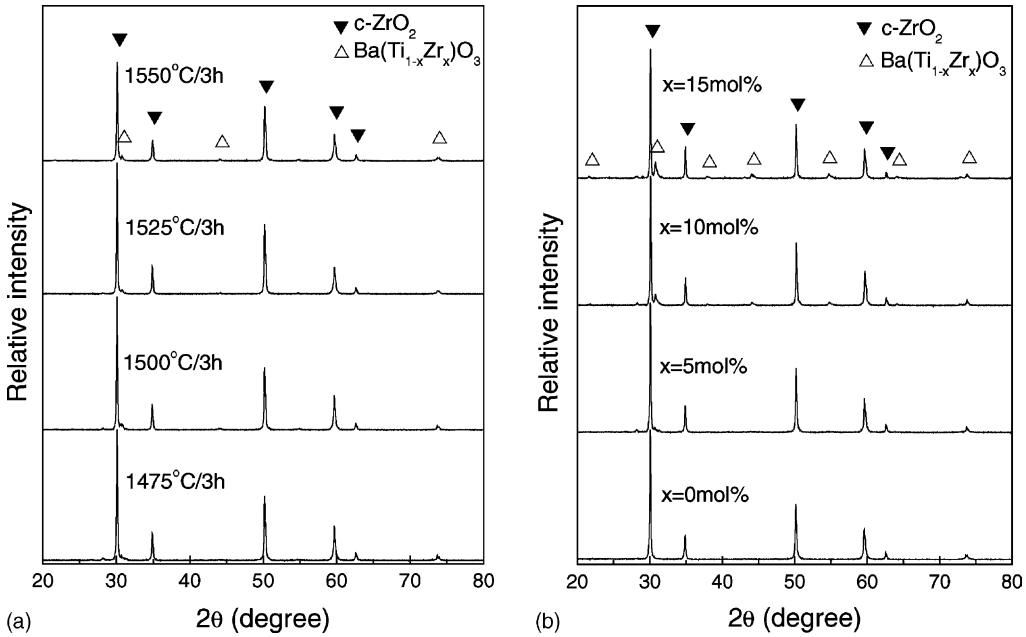

Fig. 4. XRD patterns of $0.05BaTiO_3/0.95$(8Y-FSZ) ceramics sintered under different conditions (a) and $xBaTiO_3/(1-x)$ 8Y-FSZ ceramics sintered at 1475 °C for 3 h (b).

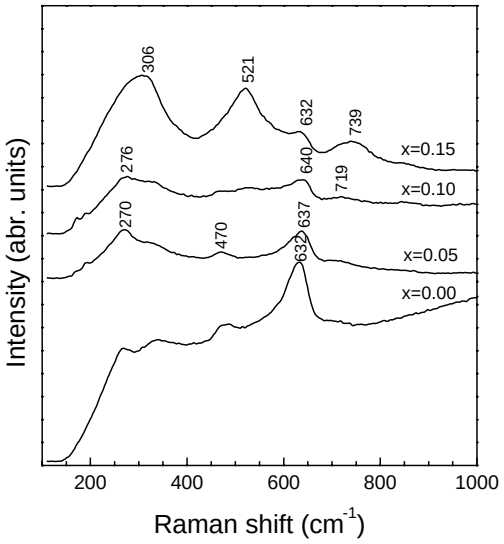

Fig. 5. Raman spectra of xBaTiO$_3$/(1 − x)8Y-FSZ ceramics sintered at 1475 °C for 3 h.

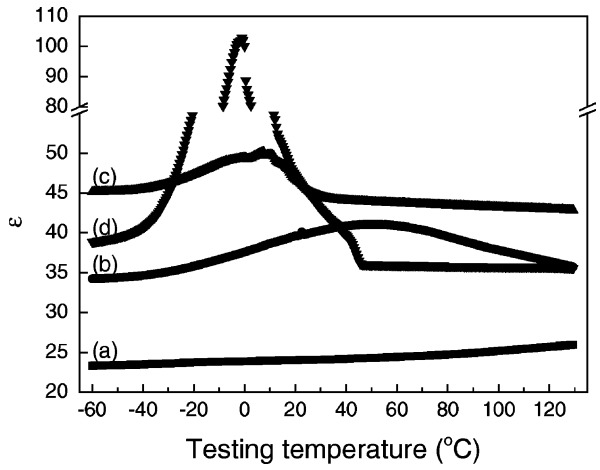

Fig. 6. Dielectric constant of xBaTiO$_3$/(1 − x)8Y-FSZ ceramics sintered at 1475 °C for 3 h at different testing temperature at 10 kHz: (a) $x = 0.00$; (b) $x = 0.05$; (c) $x = 0.10$; (d) $x = 0.15$.

x)8Y-FSZ decreases with increasing the content of additive because of the low modulus of BaTiO$_3$ phase, while the Vickers hardness increases firstly and then decreases with increasing the additive content.

The fracture toughness of xBaTiO$_3$/(1−x)8Y-FSZ ceramics sintered under different conditions is shown in Fig. 7. The fracture toughness of 8Y-FSZ ceramics is significantly enhanced by incorporating BaTiO$_3$ additive, and it reaches the maximum of 6.1 MPa m$^{1/2}$ (twice that of 8Y-FSZ matrix) at $x = 0.05$. Beyond this limit, the fracture toughness begins to decrease with a further increase of the amount of BaTiO$_3$ additive. To identify the toughening mechanisms of composite ceramics, the microstructures of ceramics should be carefully considered. As shown in Fig. 2, the fracture surface of 8Y-FSZ ceramics consists of small and uniform grains, while those of xBaTiO$_3$/(1 − x)8Y-FSZ composite

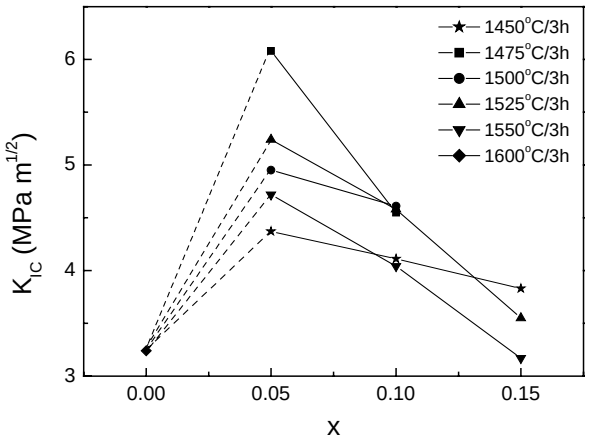

Fig. 7. Fracture toughness of xBaTiO$_3$/(1 − x)8Y-FSZ ceramics sintered under different conditions.

Table 1
Bulk densities and mechanical properties of xBaTiO$_3$/(1 − x)8Y-FSZ ceramics sintered under different conditions

Sintering conditions (°C/3 h)	Composition (x)	Density (g/cm^3)	Young's modulus (GPa)	Vickers hardness (GPa)	Fracture toughness (MPa m$^{1/2}$)
1450	0.05	5.74	133 ± 15	11.6 ± 0.3	4.4 ± 0.5
	0.10	5.74	159 ± 34	11.5 ± 0.3	4.1 ± 0.1
	0.15	5.51	185 ± 45	6.9 ± 0.1	3.8 ± 0.2
1475	0.05	5.70	176 ± 45	11.6 ± 0.8	6.1 ± 0.3
	0.10	5.63	167 ± 24	12.1 ± 0.3	4.6 ± 0.2
1500	0.05	5.68	154 ± 28	10.7 ± 0.9	5.0 ± 0.6
	0.10	5.58	147 ± 47	10.0 ± 0.2	4.6 ± 0.6
1525	0.05	5.62	143 ± 18	11.9 ± 0.3	5.2 ± 0.8
	0.10	5.50	134 ± 18	11.0 ± 0.6	4.6 ± 0.5
	0.15	5.24	115 ± 18	9.9 ± 1.5	3.6 ± 0.2
1550	0.05	5.63	131 ± 48	11.1 ± 0.6	4.7 ± 0.8
	0.10	5.52	128 ± 22	8.7 ± 0.2	4.0 ± 0.5
	0.15	5.27	90 ± 16	8.4 ± 0.1	3.8 ± 0.6
1600	0.00	5.36	149 ± 30	8.9 ± 2.8	3.2 ± 0.3

ceramics consist of mixtures of large grains and some small grains located at the grain boundaries of large grains when x is not less than 0.05, and the crack deflections should occur in these composite ceramics because of their inhomogeneous microstructures. The fracture toughness of composite ceramics is higher than the 8Y-FSZ ceramics because of the crack deflection. There are also some needle-like grains as observed in the $0.1BaTiO_3/0.9$(8Y-FSZ) ceramics, and these needle-like grains can contribute to the overall toughness via crack deflection and/or grain bridging toughening. From the above analysis, it can be deduced that the toughness of $0.1BaTiO_3/0.9$(8Y-FSZ) ceramics should be higher than that of $0.05BaTiO_3/0.95$(8Y-FSZ) ceramics because there are more active toughening mechanisms in the former than those of the latter, but in fact the fracture toughness of $0.05BaTiO_3/0.95$(8Y-FSZ) ceramics is higher than that of $0.1BaTiO_3/0.9$(8Y-FSZ), so another toughening mechanism should exist in this ceramic. Noted that the $0.05BaTiO_3/0.95$(8Y-FSZ) ceramics consists of rhombohedral ferroelectric $Ba(Ti_{1-x}Zr_x)O_3$ phase and cubic 8Y-FSZ phase, and other composite ceramics consist of non-piezoelectric cubic $Ba(Ti_{1-x}Zr_x)O_3$ phase and cubic 8Y-FSZ phase, so the high fracture toughness of $0.05BaTiO_3/0.95$(8Y-FSZ) ceramics should be due to piezoelectric/ferroelectric secondary phase toughening as shown in a previous work [3–10]. That is, the energy dissipation and/or conversion due to domain wall motion will hinder the extension of fractures and subsequently enhance the fracture toughness [3,5]. On the other hand, the fracture toughness of the composite with same composition increases with increasing sintering temperature to a maximum value and then decreases with further increasing sintering temperature. Fig. 3 shows the fracture surface of $0.05BaTiO_3/0.95$(8Y-FSZ) sintered at different temperatures for 3 h. The grain size increases with increasing temperature, and the fracture mode changes from intra- and intergranular mixed fracture to intergranular fracture. In general, for the intergranular fracture mode, the toughness will increase with the grain size, while for intragranular fracture mode, it will decrease with the grain size. In present system, the density of the composite decreases with sintering temperature, and the toughness should increase with the density. Combining the two results, the fracture toughness will increase firstly and then will decrease with increasing sintering temperature.

4. Conclusions

The $0.05BaTiO_3/0.95$(8Y-FSZ) composite consisted of cubic zirconia major phase with rhombohedral ferroelectric $Ba(Ti_{1-x}Zr_x)O_3$ secondary phase, while the cubic $Ba(Ti_{1-x}Zr_x)O_3$ secondary phase was observed together with the cubic zirconia major phase in $0.1BaTiO_3/0.9$(8Y-FSZ) and $0.15BaTiO_3/0.85$(8Y-FSZ) composites. The fracture toughness of 8Y-FSZ ceramics was significantly improved by introducing $BaTiO_3$ additive, and the optimum value of 6.1 MPa $m^{1/2}$ was obtained for $0.05BaTiO_3/0.95$(8Y-FSZ). With the $BaTiO_3$ additive higher than 5 mol%, the fracture toughness started to decrease. Moreover, the fracture toughness increased firstly and then decreased with increasing sintering temperature.

Acknowledgements

This work was supported by National Nature Science Foundation of China under grant number 59782007 and National Science Foundation for Distinguished Young Scientists under grant number 50025205.

References

[1] P.F. Becher, Microstructural design of toughened ceramics, J. Am. Ceram. Soc. 74 (1991) 255–269.
[2] A.G. Evans, Perspective on the development of high-toughness ceramics, J. Am. Ceram. Soc. 73 (1990) 187–206.
[3] X.M. Chen, B. Yang, A new approach for toughening of ceramics, Mater. Lett. 33 (1997) 237–240.
[4] B. Yang, X.M. Chen, Alumina ceramics toughened by piezoelectric secondary phase, J. Eur. Ceram. Soc. 20 (2000) 1687–1690.
[5] X.M. Chen, X.Q. Liu, F. Liu, X.B. Zhang, 3Y-TZP ceramics toughened by $Sr_2Nb_2O_7$ secondary phase, J. Eur. Ceram. Soc. 21 (2001) 477–481.
[6] Y.G. Liu, D.C. Jia, Y. Zhou, Microstructure and mechanical properties of a lithium tantalate-dispersed-alumina ceramic composite, Ceram. Int. 28 (2002) 111–114.
[7] Y.G. Liu, Y. Zhou, D.C. Jia, Q.C. Meng, Y.H. Chen, Domain switching toughening in a $LiTaO_3$ dispersed Al_2O_3 ceramic composite, Scripta Mater. 47 (2002) 63–68.
[8] S. Rattanachan, Y. Miyashita, Y. Mutoh, Microstructure and fracture toughness of a spark plasma sintered Al_2O_3-based composite with $BaTiO_3$ particulates, J. Eur. Ceram. Soc. 23 (2003) 1269–1276.
[9] A.R. Boccaccini, D.H. Pearce, Toughening of glass by a piezoelectric secondary phase, J. Am. Ceram. Soc. 86 (2003) 180–182.
[10] X.Q. Liu, X.M. Chen, Microstructure and mechanical properties of $Sr_2Nb_2O_7$-toughened 3Y-TZP ceramics, Ceram. Int. 29 (2003) 635–640.
[11] X.Q. Liu, X.M. Chen, Effects of $Sr_2Nb_2O_7$ additive on microstructures and mechanical properties of 3Y-TZP/Al_2O_3 ceramics, Ceram. Int. 28 (2002) 209–215.
[12] X.Q. Liu, X.M. Chen, Dielectric and mechanical characteristics of lanthanum aluminate ceramics with strontium niobate addition, J. Eur. Ceram. Soc. 24 (2004) 1999.
[13] N.Q. Minh, Ceramic fuel cells, J. Am. Ceram. Soc. 76 (1993) 563–588.
[14] J.P.P. Huijsmans, Ceramics in solid oxide fuel cells, Curr. Opin. Solid State Mater. Sci. 5 (2001) 317–323.
[15] M. Takeuchi, O_2 sensor, Bull. Ceram. Soc. Jpn. 17 (1982) 433–438.
[16] A. Selcuk, A. Atkinson, Strength and toughness of tape-cast yttria-stabilized zirconia, J. Am. Ceram. Soc. 83 (2000) 2029–2035.
[17] Y. Ji, J. Liu, Z. Lu, X. Zhao, T. He, W. Su, Study on the properties of Al_2O_3-doped $(ZrO_2)_{0.92}(Y_2O_3)_{0.08}$ electrolyte, Solid State Ionics 126 (1999) 277–283.
[18] N. Bamba, Y.H. Choa, T. Sekino, K. Niihara, Microstructure and mechanical properties of yttria stabilized zirconia/silicon carbide nanocomposites, J. Eur. Ceram. Soc. 18 (1998) 693–699.

[19] B. Yang, X.M. Chen, X.Q. Liu, Effect of $BaTiO_3$ addition on structures and mechanical properties of 3Y-TZP ceramics, J. Eur. Ceram. Soc. 20 (2000) 1153–1158.
[20] D.B. Marshall, T. Noma, A.G. Evans, A simple method for determining elastic-modulus-to-hardness ratios using Knoop indentation measurements, J. Am. Ceram. Soc. 65 (1982) C175–C176.
[21] A.G. Evans, E.A. Charles, Fracture toughness determinations by indentation, J. Am. Ceram. Soc. 59 (1976) 371–372.
[22] K. Niihara, R. Morena, D.P.H. Hasselman, Evaluation of K_{1C} of brittle solids by the indentation method with low crack-to-indent ratios, J. Mater. Sci. Lett. 1 (1982) 13–16.
[23] A. Feinberg, C.H. Perry, Structural disorder and phase transitions in ZrO_2–Y_2O_3 system, J. Phys. Chem. Solids 42 (1981) 513–518.
[24] P.S. Dobal, A. Dixit, R.S. Katiyar, Z. Yu, R. Guo, A.S. Bhalla, Micro-Raman scattering and dielectric investigations of phase transition behavior in the $BaTiO_3$–$BaZrO_3$ system, J. Appl. Phys. 89 (2001) 8085–8091.
[25] R. Farhi, M. El Marssi, A. Simon, J. Ravez, A Raman and dielectric study of ferroelectric $Ba(Ti_{1-x}Zr_x)O_3$ ceramics, Eur. Phys. J. B 9 (1999) 599–604.